during the clear weather tests of December 6. These showed the CPR levels associated with off-axis reception to be well below the values measured during the storm (at least for the high residual CPR associated with $\theta = -16.5°$) and would seem to eliminate off-axis reception as a source of error in our data.

A striking feature of the snow data displayed in Fig. 6 compared to rain data from a terrestrial link [2] is the large depolarization observed for a given attenuation. To get a CPR of −28 dB (the leftmost $\theta = -19.5°$ point in Fig. 6) with rain on a ground path would require at least 7-dB attenuation and possibly as much as 20 or 30 dB, depending on path length and raindrop canting angle.

Some theoretical case may be made for associating small attenuation and severe depolarization with scattering by bodies which are relatively lossless but lack rotational symmetry. Certainly snowflakes and high-altitude ice crystals fit this description, but the very fragmentary data available for snow do not necessarily support this conclusion. Watson [11] working at 11 GHz with a 13.7-km path reported a huge fade (24 dB) in wet snow accompanied by a CPR of −22 dB. On the other hand, a rain fade of only 8 dB on the same path was associated with a −20-dB CPR. Since our frequency is almost twice that of Watson's and his snow was wet while ours was dry, it is very possible that he could have been dealing with scatterers that were relatively more isotropic than ours were. Some Russian work [12] at a much higher frequency also indicates that, for the same water content, snow attenuates more highly than rain, but this tells us nothing about depolarization. Clearly more research is needed. We should operate a terrestrial path link and a satellite downlink simultaneously, and also study the high-altitude conditions with a polarization diversity radar.

ACKNOWLEDGMENT

The authors wish to thank C. C. Hupfeld, W. W. Farley, Jr., S. R. Kauffman, and H. N. Pendrak for their help in acquiring the data presented here. They would also like to recognize the assistance of S. R. Kauffman and S. Johnson in reducing the data and preparing the manuscript for publication.

REFERENCES

[1] P. A. Watson, "Crosspolarization isolation and discrimination," *Electron. Lett.*, vol. 9, pp. 516–517, Nov. 1973.
[2] C. W. Bostian, W. L. Stutzman, P. H. Wiley, and R. E. Marshall, "The influence of polarization on millimeter wave propagation through rain," Dep. Elec. Eng., Virginia Polytechnic Institute and State Univ., Blacksburg, NASA Grant NGR-47-004-091, Final Rep., Jan. 1974. (Available from NTIS as NASA CR-143686.)
[3] P. A. Watson and M. Arbabi, "Rainfall cross polarization at microwave frequencies," *Proc. Inst. Elec. Eng.*, vol. 120, pp. 413–418, Apr. 1973.
[4] P. H. Wiley, W. L. Stutzman, and C. W. Bostian, "A new model for rain depolarization," *J. Rech. Atmos.*, vol. 8, pp. 147–153, Jan.–June 1974.
[5] R. R. Taur, "Rain depolarization: Theory and experiment," *COMSAT Tech. Rev.*, vol. 4, pp. 187–190, Spring 1974.
[6] D. A. Gray, "Depolarization of ATS-6 satellite 20 GHz beacon transmitted through rain," in *USNC/URSI June 1975 Meeting Abstracts*, Urbana, Ill., p. 30.
[7] D. C. Cox, "Design of the Bell Laboratories 19 and 28 GHZ satellite beacon propagation experiment," in *IEEE 1974 ICC Dig.*, June 1974.
[8] S. I. Ghobrial and P. A. Watson, "Cross polarization during clear weather conditions," presented at the Inst. Elec. Eng. Conf. Propagation of Radio Waves at Frequencies Above 10 GHz (Inst. Elec. Eng. Conf. Publ. 98).
[9] C. W. Bostian, W. L. Stutzman, P. H. Wiley, and R. E. Marshall, "Initial results of an experimental study of 17.65 GHz rain attenuation and depolarization," in *1972 Int. IEEE G-AP Symp. Dig.* (1972), pp. 250–253.
[10] C. W. Bostian, "Antenna and path interaction in rain depolarization," in *1974 Int. IEEE AP-s Symp. Dig.* (1974), pp. 392–394.
[11] P. A. Watson *et al.*, "Cross polarization studies at 11 GHz," Univ. Bradford, Bradford, England, Final Rep. European Space Res. Organization Contract 1247/SL, June 1973.
[12] Yu. S. Babkin *et al.*, "Attenuation of radiation at wavelength of 0.96 mm in snow," *Radio Eng. Electron. Phys.* (USSR), vol. 15, pp. 2171–2174, 1970.

Microwave Scattering from the Ocean Surface

W. LINWOOD JONES,
WILLIAM L. GRANTHAM, MEMBER, IEEE,
LYLE C. SCHROEDER, JAMES W. JOHNSON,
CALVIN T. SWIFT, SENIOR MEMBER, IEEE,
AND JOHN L. MITCHELL

***Abstract*—This paper reviews current aircraft and satellite programs which use microwaves to measure ocean wave and surface wind conditions. These particular measurements have been identified by the user community as offering significant economic and technological benefits. Active microwave remote sensing techniques for these applications have been described theoretically and verified experimentally. The results of recent aircraft and satellite experimental programs are presented herein along with plans for the SeaSat-A satellite scatterometer (SASS).**

INTRODUCTION

For many years many industrial and government groups have expressed interest in measuring a variety of oceanographic conditions. However, the great area of the sea and its harsh environment have prevented effective monitoring with sufficient observational density to satisfy most of their requirements. A recent study conducted for NASA has shown that significant economic and technological benefits would result from a satellite able to measure ocean waves and surface winds on a global scale. Even though many desired oceanographic parameters cannot be inferred from satellite measurements, data from a spacecraft can be combined with other surface measurements to construct a more general view of the ocean. Furthermore, surface observations are quite useful by themselves to bolster the library of measurements of the ocean/atmosphere interaction. Several active microwave techniques have been shown, both theoretically and experimentally, to be applicable for aircraft and/or satellite ocean measurements. Other radar techniques in earlier stages of development promise improved or expanded ocean remote sensing capabilities. This short paper reviews several of the foregoing techniques including recent aircraft and satellite ocean measurements and presents plans for the SeaSat-A satellite scatterometer (SASS).

WAVE MEASUREMENTS

An extensive real-time data collection network with rapid dissemination of data to users does not currently exist for the global ocean wave conditions. Moreover, existing quantitative techniques utilize *in situ* instrumentation and frequently involve laborious data analyses. Radar techniques, however, have exhibited potential for rapid and accurate measurements of ocean wave conditions over large areas.

A dual-frequency correlation technique has been developed by Weissman [1] for measuring the root-mean-square (rms) wave height averaged over an area of the sea that is much greater than typical horizontal wavelengths, of the wind-generated waves. Implementation of this technique on commercial and/or military aircraft while on transoceanic flights would provide routine observations of rms wave height over major shipping lanes. This technique of measurement involves a near-nadir looking radar that transmits and then receives two monochromatic plane electromagnetic waves simultaneously. At the receiver the two radar returns are correlated as a function of their variable frequency separation Δf. The resulting cross correlation $R(\Delta f)$ depends primarily on the rms wave height.

Manuscript received April 14, 1975; revised August 13, 1975.

W. L. Jones, W. L. Grantham, L. C. Schroeder, J. W Johnson, and C. T. Swift are with the Langley Research Center, National Aeronautics and Space Administration, Hampton, Va. 23665.

J. L. Mitchell is with the LTV Aerospace Corporation, Hampton, Va. 23665.

However, Barrick [2] has shown that for targets distributed on a plane, $R(\Delta f)$ varies with the incidence angle of these plane waves, and for the configurations that arise in microwave backscattering from the ocean, this variation is very strong. Therefore, the beamwidths and patterns of the transmitting and receiving antennas are an important factor and must be considered in studying the capabilities and resolution of this technique. Weissman's analysis [1] concludes that the pattern effect can be adequately predicted, and the resultant equation for the magnitude of the two-frequency correlation coefficient is

$$|R(\Delta f)| = \exp\left[-2(2\pi\Delta f/c)^2\sigma^2\right] \quad (1)$$

where

σ rms wave height;
θ antenna beamwidth;
C speed of light;
$P(\Delta f,\theta)$ antenna pattern decorrelation factor.

The $P(\Delta f,\theta)$ term adversely affects the sensitivity in the measurement of σ; therefore, it should be minimized by minimizing θ.

The two-frequency correlation technique requires that two narrowband signals (one with variable frequency) be simultaneously transmitted and that the returns be separated and their complex amplitudes correlated. For aircraft implementation of this technique at ground speeds less than 100 m/s and altitudes up to approximately 3300 m, consecutive measurements made within 1 ms may be considered to be simultaneous. An aircraft instrument, the dual-frequency scatterometer (DFS), was designed and developed consistent with these requirements and flight tested by the NASA Langley Research Center (LaRC) in 1974.

The DFS is a modification of an existing scatterometer and many of its operational characteristics were dictated by the parent instrument. A simplified block diagram of those portions of the instrument peculiar to DFS is shown in Fig. 1. The operating frequency is selected on a pulse-by-pulse basis (every 80 μs) by switching between two phase-locked oscillators f_a and f_b. The frequency of the f_a oscillator is fixed at 13.9 GHz and f_b is selectable to yield 13.9 GHz $-$ Δf, where Δf ranges from 1–40 MHz. The value of Δf is stepped sequentially in as many as 16 increments with a minimum increment of 1 MHz. The returned pulses are amplitude detected, ac coupled, and alternately sampled, thereby separating the amplitude modulation of the f_a return signal, v_a, and the f_b return, v_b. Weissman [3] has shown that

$$|R(\Delta f)|^2 \alpha \langle v_a v_b \rangle \quad (2)$$

where the brackets denote time averaging. The quantity $\langle v_a v_b \rangle$ is produced at the DFS correlator along with appropriate normalizing factors so that minimal data analysis is required to infer σ from the measurement using (1).

Aircraft measurements have been made under low-, moderate-, and high-sea state conditions. Predominantly, these measurements

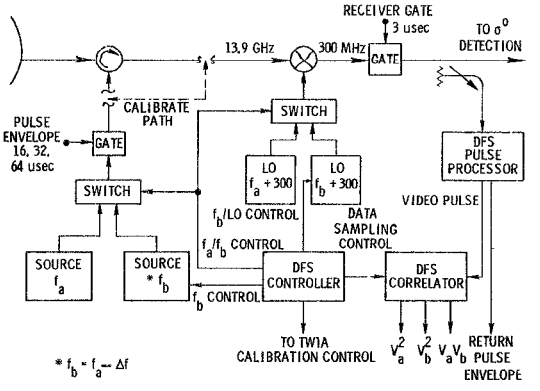

Fig. 1. Block diagram of dual frequency scatterometer.

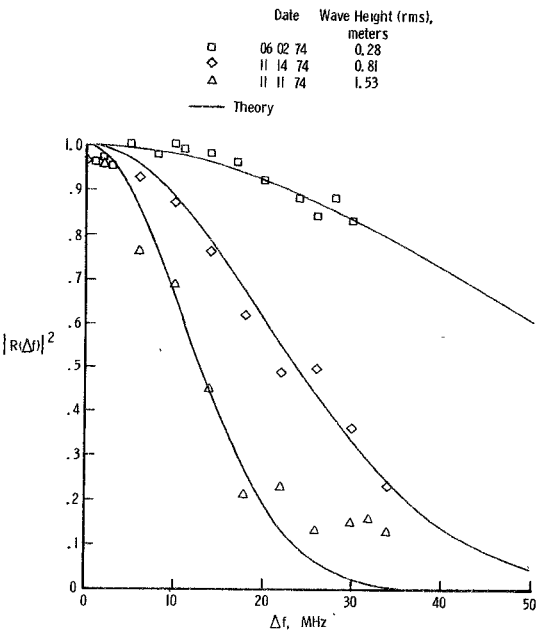

Fig. 2. Dual frequency scatterometer correlation coefficient for low-, moderate-, and high-sea states from aircraft at 3048-m altitude.

have been made from an altitude of 3048 m with a 1.5° antenna beamwidth. Under these conditions, the diameter of the illuminated surface area was approximately 80 m. Results reported by Johnson [4] for low- and moderate-sea states were in good agreement with Weissman's theory. Additional measurements with significant wave heights up to 6.5 m (Fig. 2) also showed good agreement for low- and moderate-sea states. The high-sea state data however showed significant deviations from theory. In this case, preliminary wave measurements using an aircraft laser profilometer indicate the dominant water wavelength to be in the neighborhood of 160 m. Thus it is hypothesized that the effect seen in Fig. 2 for high-sea states and large values of Δf is the result of an inadequate number of scattering points in the antenna footprint. In Fig. 2, the rms wave height σ is a calculated best fit to the data. Laser profilometer wave data were taken on these flights and are currently being processed to yield rms wave height for comparison with the radar inferred values.

Tomiyasu [5] has proposed a short-pulse wave directional-spectrometer approach whereby the time-varying amplitude of the backscattered signal is used to infer the directional wave slope spectrum. A short transmitted pulse sweeps across the ocean surface producing a backscatter signal that is essentially the impulse response of the waves. An ocean wave spectrum can then be resolved by signal processing. Short-pulse radar measurements were made in the North Sea by the Naval Research Laboratory (NRL) during the fall of 1973 with data analysis provided by the NASA Goddard Space Flight Center (GSFC). The NRL instrument operated at 9.75 GHz with a 12.5-ns pulse length and antenna beamwidths broad enough to ensure pulse-limited conditions. Fig. 3 shows wave-directional spectrometer results for a 10° incidence angle, 3350-m altitude, and 6-m/s surface wind speed compared with accompanying laser profilometer and radar altimeter measurement results. Development of this technique is being pursued by NASA-GSFC in cooperation with NRL, and the idea has been conceptually developed into a satellite ocean wavelength sensor by Eckerman [6].

WIND VECTOR MEASUREMENTS

During the period 1965–1971, extensive measurements of the radar backscatter from the ocean were performed by personnel of the Naval Research Laboratory. The system used was the NRL four-frequency airborne coherent pulsed radar operating at 428 MHz, 1228 MHz, 4455 MHz, and 8910 MHz. The antenna system was composed of

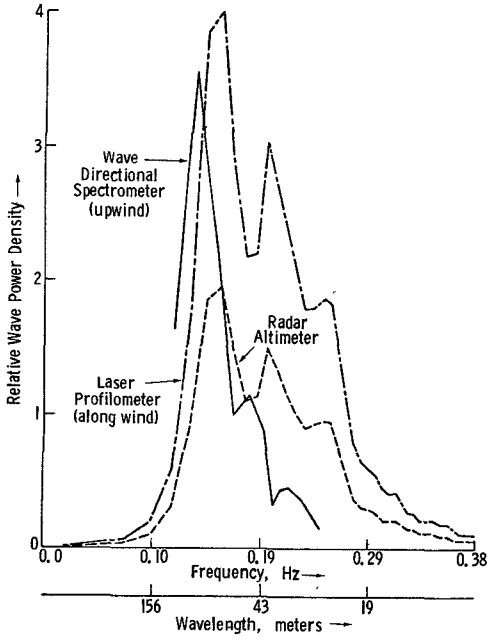

Fig. 3. North Sea wave height spectra by NRL at a wind speed of 6 m/s.

four dual linear-polarized antennas which were sequentially used in all combinations at each frequency. The antennas were stabilized in roll and pitch and could mechanically scan through 315° in azimuth and 100° in elevation. A dual channel receiver (direct and cross polarized) measured both the amplitude and phase of the backscattered signal for the polarization combinations.

Typical system operating parameters were: peak power, 25 kW; pulse repetition rate, 500–800 Hz; pulse length, 0.25–0.5 μs; IF bandwidth, 10 MHz; and range gate width, 25–50 ns. The received power from the ocean was absolutely calibrated by referencing it to the power returned from aluminum spheres dropped from the aircraft. This method of system calibration has been described by Guinard and Daley [7] and the results of the aforementioned programs have been published by Valenzuela *et al.* [8] and Daley [9]. A comprehensive data bank has been established on the parametric behavior of the normalized radar scattering coefficient σ^0 as a function of radar wavelength, polarization, and incidence angle for a variety of sea and wind conditions ranging from calm to rough seas (7–8-m wave heights) and high winds (24 m/s).

Other aircraft measurements of ocean radar scattering coefficient were obtained by the NASA Johnson Space Center (JSC) using a 13.3-GHz continuous-wave Doppler radar scatterometer. This system used two fan-beam antennas (separate transmitting and receiving) to radiate a wide (120°) beamwidth fore and aft and a narrow (3°) beamwidth across the flight path. Two 13.3-GHz scatterometers were used, which were similar, except one was vertically polarized and the other was dual, linearly polarized. The receiver was a homodyne type with both in-phase and quadrature channels. The composite baseband video spectrum was recorded on magnetic tape and was later processed to yield σ^0 for incidence angles between ±60° (near-nadir data were excluded). Flights were conducted under a variety of sea-state and surface wind conditions, and the radar signatures were characterized according to ocean surface conditions [10]–[12].

An analysis of NRL and NASA-JSC data has been performed by Apel [13] to determine the dependence of ocean σ^0 on surface wind speed. To remove instrument biases, σ^0 at 35° incidence was normalized to σ^0 at 10° incidence (theoretical incidence angle for minimum ocean σ^0 variation). When these data are plotted as in Fig. 4, the result suggests a power-law relationship such that

$$\sigma^0 = AU^\nu \tag{3}$$

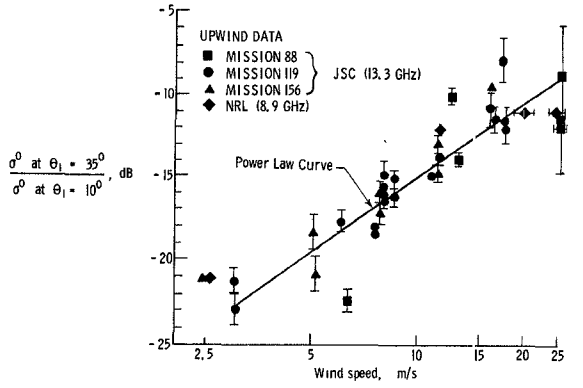

Fig. 4. Normalized scattering coefficient data from JSC and NRL.

TABLE I
TABLES OF WIND-SPEED POWER COEFFICIENT

Freq.	Direction	Polarization	Exponent	Incidence Angle 20°	25°	30°	40°	50°
8.9 GHz	Upwind	VV	ν	0.20	0.25	0.27	0.66	0.73
	Downwind	VV	ν	0.20	0.29	0.36	0.80	0.80
	Upwind	HH	ν	0.00	0.33	0.58	0.87	1.03
	Downwind	HH	ν	0.00	0.29	0.52	1.04	1.30

(a) NRL

Freq.	Direction	Polarization	Exponent	Incidence Angle, θi 25°	35°
13.3 GHz	Upwind	VV	ν	1.12	1.49
	Downwind	VV	ν	1.15	1.60
	Crosswind	VV	ν	1.00	1.40

(b) NASA-JSC

Freq.	Direction	Polarization	Exponent	Incidence Angle, θi 20°	30°	40°	50°
13.9 GHz	Upwind	VV	ν	1.65	1.68	1.77	1.66
	Downwind			.98	1.56	1.62	1.55
	Crosswind			.98	1.49	1.52	1.51
13.9 GHz	Upwind	HH	ν	1.00	1.65	1.98	1.93
	Downwind			.94	1.68	1.97	1.96
	Crosswind			.75	1.45	1.46	1.48

(c) AAFE RADSCAT

where

A a constant;
U wind speed;
ν the wind-speed power coefficient.

Fitting (3) to the data leaves large residuals (Fig. 4) and controversy exists as to whether or not σ^0 becomes constant for high wind speeds. Better power-law fits were obtained for each data set separately. Listings of wind-speed power coefficients for upwind, downwind, and crosswind observations have been obtained for NRL data from Daley [9] and for NASA-JSC data from Bradley [11] and Claassen [12] and are listed in Table I(a) and (b).

To help resolve differences in NRL and NASA-JSC wind-speed power coefficients, measurements were obtained by NASA-LaRC [14], [15] using a 13.9-GHz pencil-beam scatterometer (AAFE RADSCAT). This instrument consisted of a high-precision long-pulse (interrupted CW) microwave scatterometer, mounted in the NASA-JSC C-130 aircraft. The antenna looked out of the open ramp of the C-130, so that the radar obtained an unobstructed view of the ocean's surface without the use of a radome. A dual linear-polarized parabolic antenna was mechanically scanned in elevation to view the

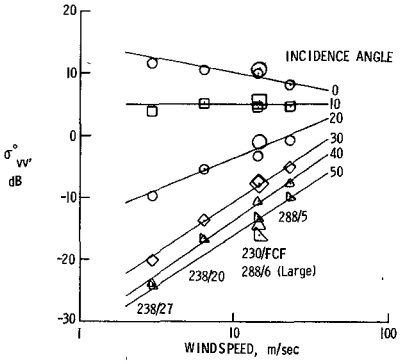

Fig. 5. Downwind σ^0_{VV} versus wind speed.

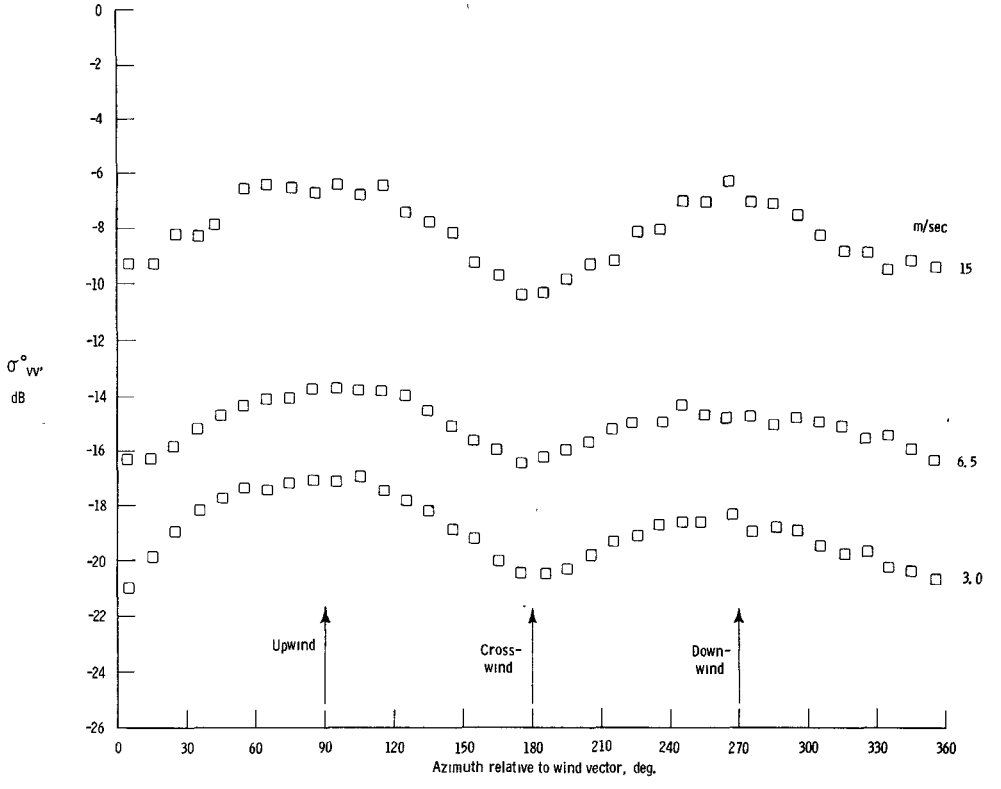

Fig. 6. AAFE RADSCAT scatterometer wind direction sensitivity.

surface from nadir to approximately 55° aft. Radar measurements were obtained for vertical and horizontal polarizations as a function of incidence angle and flight direction over a range of wind speeds from 3 m/s to 28 m/s. Fig. 5 shows a plot of downwind σ^0 versus wind speed for various incidence angles, and the corresponding wind-speed power coefficients are also tabulated in Table I(c).

Previous observations by NRL and NASA-JSC indicated an azimuthal variation (wind direction dependence) of the scattering coefficient for incidence angles well off nadir. To examine this effect, the AAFE RADSCAT antenna was pointed perpendicular to the aircraft pitch and longitudinal axis, and the aircraft was flown in circles.

Surface wind vector measurements were made at these sites before and after radar scatterometer measurements. The aircraft was flown at low altitude (100–150 m) in the nominal upwind and downwind directions for periods of about 5 min, and wind-speed and direction measurements were made using the aircraft inertial navigation system. Wind vector measurements for Skylab underflight missions (flights designated M238/F20 and M238/F27 on Fig. 6) were supplied by NOAA aircraft using an AWARS navigation system. Measurements for all other missions on Fig. 6 were obtained by the NASA C-130 aircraft, using a Litton LTN-51 navigation system. Wind vector accuracy for the NOAA system is ± 1 m/s $\pm$ 10° and for the NASA system the accuracy is ± 1.5 m/s $\pm$ 10°.

Wind direction measurements made by the aircraft were assumed to be the same as at the standard 19.5-m altitude, but wind-speed measurements were extrapolated to this altitude using a wind profile method described by Cardone [16].

The dependence of vertical polarization σ^0 on wind azimuth is shown for three wind speeds in Fig. 6. These data demonstrate the potential for remote sensing of wind speed and direction and are the basis for a proposed wind vector sensor to be flown on the SeaSat-A satellite.

The first satellite measurements of ocean scattering coefficient were obtained during the NASA-JSC manned space flight Skylab program. The Skylab earth resources package contained a mechanically scanned pencil-beam 13.9-GHz scatterometer (similar to AAFE RADSCAT) known as S-193 RADSCAT. Data from this instrument were taken during the Skylab II, III, and IV missions (June 1973–February 1974). Aircraft underflights to obtain "ground

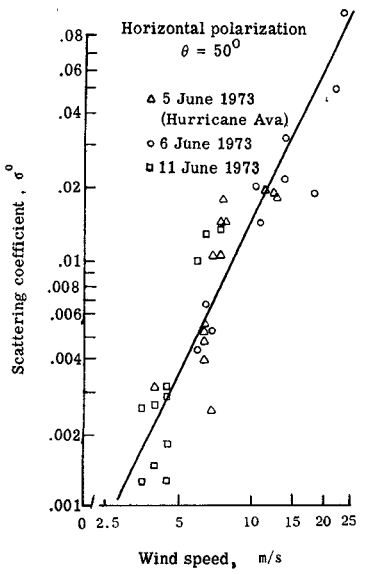

Fig. 7. Skylab S-193 scatterometer response: wind at sea.

truth" measurements were also flown for many of the Skylab missions. These Skylab data are under analysis by many researchers [17]–[19]. Preliminary results [17] of ocean scattering coefficient versus wind speed are shown in Fig. 7 for a 50° incidence angle. The wind-speed data were derived from metoerological analysis (see [17]). These data, as well as results at other incidence angles and both polarizations, support the aircraft-measured backscattering power-law response to wind speed.

FUTURE SATELLITE SCATTEROMETER MEASUREMENTS

Future applications of microwave scatterometry will provide measurement of ocean surface wind speed and direction for the NASA SeaSat-A oceanographic satellite (1978 launch). Specifications for the scatterometer have been developed based on requirements of the SeaSat User Working Group (UWG): viz., wind-speed measurement range of 3–50 m/s with an accuracy of ±2 m/s or ±10 percent whichever is greater; wind direction 0–360° ± 20°; 1000-km swath; 50-km resolution cell; cross-track and along-track spacing between resolution cells of 100 km.

From a number of scatterometer design options ranging from pencil beam to fan beam, the fan-beam approach was chosen. As discussed by Grantham *et al.* [20], four antennas will be used to produce a star-like illumination on the earth's surface (Fig. 8), and, as the satellite orbits the earth, this star pattern will cut a swath 761 km wide on each side of the satellite subtrack. The illuminated footprints will be subdivided into small resolution cells using Doppler filtering to obtain a 50-km-resolution cell size.

The primary swath is 500 km wide on each side of the subtrack and is bounded on the inside by an incidence angle of 25°. Smaller angles are excluded because the radar return becomes insensitive to surface winds at angles below about 20°. The outer boundary of the primary swath is at a 55° incidence angle, the outer limit of present comprehensive scatterometer data. Recent scatterometer data taken from the JSC C-130 aircraft show the scattering coefficient to be sensitive to wind vector out to at least 60° incidence. An additional high-wind-speed zone between 55° and 65° incidence angle is therefore included, and return signals should be large enough to measure if the winds exceed 10 m/s.

Although the scattering coefficient is a function of wind direction as well as wind speed (Fig. 6), it has been determined [20] that two measurements are adequate to determine wind vector at each resolution cell. An optimum implementation is a forward- and aft-looking beam (Fig. 8), providing two measurements separated in azimuth by

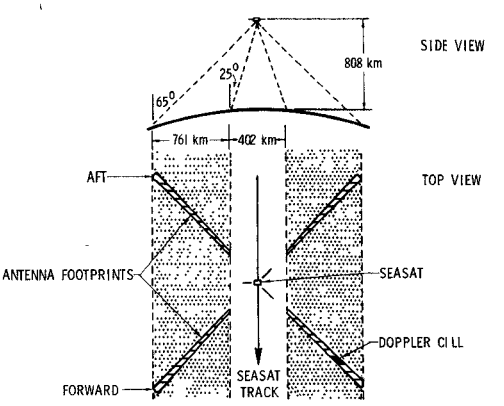

Fig. 8. Earth-satellite geometry for SeaSat scatterometer.

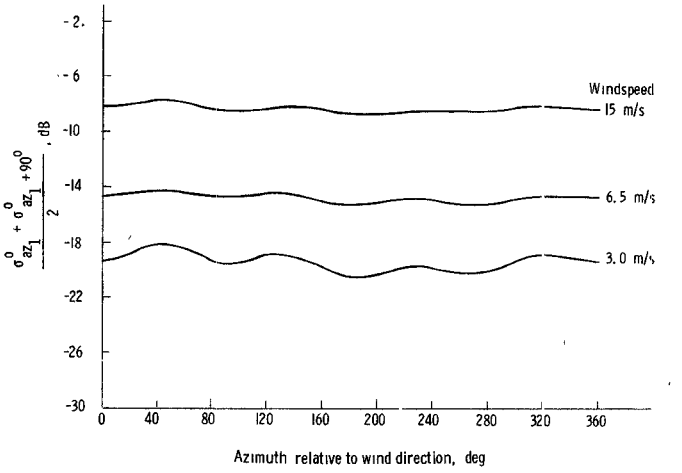

Fig. 9. Mean σ^0_{VV} at two orthogonal wind azimuths. From AAFE RADSCAT data at 30° incidence.

90° at each resolution cell. The mean of these two measurements is a strong function of wind speed but nearly independent of wind direction. This is demonstrated in Fig. 9, where this mean has been plotted for the data of Fig. 6. After determining wind speed using this mean σ^0 value, wind direction can be determined by curve fitting the two σ^0 measurements to a previously determined experimental curve for that wind speed and incidence angle. This wind direction information can be used if necessary to iterate to an improved wind-speed accuracy.

From the surface wind data obtained using the scatterometer, synoptic wind fields can be computed and used in long-range weather and sea state forecasting.

ACKNOWLEDGMENT

The authors wish to thank A. E. Cross for assistance in figure preparation.

REFERENCES

[1] D. E. Weissman, "Two frequency radar interferometry applied to the measurement of ocean wave height," *IEEE Trans. Antennas Propagat.*, vol. 21, pp. 649–656, Sept. 1973.
[2] D. E. Barrick, "Determination of rms height of a rough surface using radar waves," Antenna Lab., Ohio State Univ., Columbus, Rep. 1388-19, Aug. 1965.
[3] D. E. Weissman *et al.*, "A dual frequency radar for ocean roughness sampling," presented at the URSI Specialist Meeting Microwave Scattering and Emission from the Earth, Berne, Switzerland, Sept. 1974.
[4] J. W. Johnson *et al.*, "Dual frequency scatterometer measurement of ocean wave height," presented at the 1974 USNC/URSI Meeting, Boulder, Colo., Oct. 1974.

[5] K. Tomiyasu, "Short pulse wide-band Scatterometer ocean surface signature," *IEEE Trans. Geosci. Electron. (Special Issue on Remote Sensing)*, vol. GE-9, pp. 175–177, July 1971.
[6] J. Eckerman, "Satellite instrumentation for ocean surface measurements," presented at the 1974 IEEE INTERCON, New York, Mar. 26–29, 1974.
[7] N. W. Guinard and J. C. Daley, "An experimental study of sea clutter model," *Proc. IEEE*, vol. 58, pp. 543–550, Apr. 1970.
[8] G. R. Valenzuela, M. B. Laing, and J. C. Daley, "Ocean spectra for the high frequency waves as determined from airborne radar measurements," *J. Marine Res.*, vol. 29, no. 2, 1971.
[9] J. C. Daley, "An empirical sea clutter model," NRL Memo Rep. 2668, Dec. 1973.
[10] K. Krishen, "Correlation of radar backscattering cross sections with ocean wave height and wind velocity," Lockheed Electronics Co., Houston, Tex., TR 649D. 21.025, March 1970.
[11] G. A. Bradley, "Remote sensing of ocean winds using a radar scatterometer," Ph.D. dissertation, Univ. Kansas Center for Research, Inc., 1971.
[12] J. P. Claassen and H. S. Fung, "The wind response of radar sea return and its implication on wave spectral growth," Univ. Kansas Center for Research, Inc., Tech. Rep. 186-5, Sept. 1971.
[13] J. R. Apel, "A hard look at oceans from space," presented at the AIAA 9th Annu. Meeting, Washington, D. C., Jan. 8–10, 1973, Paper no. 73-11.
[14] C. T. Swift and W. L. Jones, "Satellite radar scatterometry," presented at the 1974 IEEE INTERCON, New York, Mar. 26–29, 1974.
[15] W. L. Jones, W. L. Grantham, L. C. Schroeder, and J. L. Mitchell, "Microwave scatterometer measurements of ocean wind vector," presented at the 1974 USNC/URSI Meeting, Boulder, Colo., Oct. 1974.
[16] V. J. Cardone, "Specification of the wind distribution in the marine boundary layer for wave forecasting," New York Univ., School of Engineering and Science, New York, Mar. 1970, Rep. TR69-1 (available as DDS no. AD702 490).
[17] R. K. Moore *et al.*, "Simultaneous active and passive microwave response of the earth—The Skylab RADSCAT experiment," in *Proc. 9th Symp. Remote Sensing of the Environment* (Ann Arbor, Mich., April 1974).
[18] D. Ross *et al.*, "Remote sensing of pacific hurricane and radiometric measurements from foam and slicks," NOAA, Miami, Fla., Progress Rep. NASA CR 140126, July 31, 1974.
[19] A. K. Jordan, C. G. Purves, and J. F. Diggs, "Analyses of Skylab II S-193 scatterometer data," NRL Rep. 7877, May 2, 1975.
[20] W. L. Grantham *et al.*, "An operational satellite scatterometer for wind vector measurements over the ocean," NASA TM-X 72672, Mar. 1975.

Microwave Irradiation Design Using Dielectric Lenses

HENRY S. HO, MEMBER, IEEE, GARY J. HAGAN, AND MARK R. FOSTER

***Abstract*—Theoretical calculations and electric-field measurements were made to investigate the focusing effects of plane-wave-irradiated dielectric spheres (lenses). Spheres of different diameters and dielectric properties and plane wave sources of different frequencies were used in the calculations. The results indicate the feasibility of using dielectric lenses for selective partial-body irradiation in biological experiments.**

INTRODUCTION

The use of concentrated microwave beams for communication between distant stations has been widely investigated, resulting in dramatic advances in modern antenna and radar designs. However, in the area of biological researches and medical applications of microwaves, it may be desirable to focus microwave energy in a very small region in the proximity of the focusing lens. One application of this technique involves the selective heating of rabbit eyes with a dielectric lens for microwave cataractogenesis experiments [1].

In the current investigation, theoretical calculations and electric-field measurements are made to determine the focused effects of electric fields behind a plane-wave-irradiated dielectric sphere (lens) [2], [3]. Parameters for this investigation include sizes and dielectric properties of the sphere and the frequency of the incident plane wave.

CALCULATIONS OF ELECTROMAGNETIC FIELDS BEHIND A PLANE-WAVE-IRRADIATED DIELECTRIC SPHERE

The formulation for the scattered electromagnetic fields from a plane-wave-irradiated dielectric sphere has been reported by Stratton [4]. The total field at a location is therefore the summation of the incident plane-wave field and the scattered field at that location. Based on this formulation, a computer program is written to calculate the electric field patterns behind a plane-wave-irradiated dielectric sphere. The direction of the electric field behind the dielectric sphere is also determined. Fig. 1 shows a plane-wave-irradiated dielectric sphere with a set of rectangular coordinates. An X–Y plane is shown behind the dielectric sphere. The electric fields squared on X–Y, X–Z, and Y–Z planes are calculated and presented in "three-dimensional" plots. The electric fields squared on all the planes are normalized to the incident plane-wave electric field squared. The magnitude of the peak of the normalized electric-field-squared pattern on each X–Y plane is defined as the focusing factor on the plane. The focusing factor of each X–Y plane depends on the distance of the plane behind the dielectric sphere. Eight different sphere sizes, three different dielectric materials, and two source frequencies are used for the calculation. The sphere diameters range from 5.1 cm through 40.6 cm. The dielectric materials are polyethylene ($\epsilon' = 2.26$, $\tan\delta = 3.6 \times 10^{-4}$), polyfoam ($\epsilon' = 1.98$, $\tan\delta = 7.0 \times 10^{-4}$), and Emerson and Cumings, Inc. Stycast 35 DA ($\epsilon' = 5.0$, $\tan\delta = 10 \times 10^{-4}$). The source frequencies are 2450 MHz and 10 GHz.

RESULTS OF THEORETICAL CALCULATIONS

Fig. 2(a) shows the normalized electric-field-squared pattern in a 40-cm × 40-cm X–Y plane at the location of maximum focusing behind a 20.3-cm-diam polyfoam sphere which is irradiated by a 2450-MHz plane wave. The plane is located directly behind the sphere at $d = 0$ cm because the focal point is inside the sphere. The patterns of the normalized electric field squared on 40-cm × 20-cm X–Z and Y–Z planes for the same 20.3-cm-diam polyfoam sphere and 2450-MHz incident plane wave are shown in Fig. 2(b), (c). These patterns show a gradual decrease of the peak of the focused

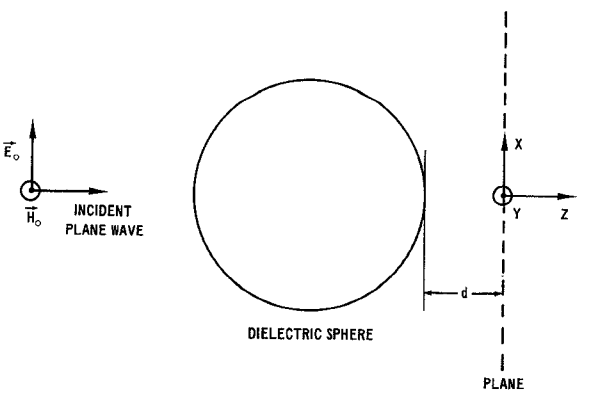

Fig. 1. An X–Y plane behind a dielectric sphere irradiation by an electromagnetic plane wave. Characters with arrows in figure appear as boldface italic in text.

Manuscript received April 18, 1975; revised August 15, 1975.
The authors are with the Division of Biological Effects, Bureau of Radiological Health, Food and Drug Administration, Public Health Service, U. S. Department of Health, Education, and Welfare, Rockville, Md. 20852.